THE JOURNAL OF PHYSICAL CHEMISTRY C

C: Energy Conversion and Storage; Energy and Charge Transport

Distinction Between Intrinsic and X-ray Induced Oxidized Oxygen States in Li-Rich 3d Layered Oxides and LiAlO

Zachary W. Lebens-Higgins, Julija Vinckeviciute, Jinpeng Wu, Nicholas V. Faenza, Yixuan Li, Shawn Sallis, Nathalie Pereira, Ying Shirley Meng, Glenn G. Amatucci, Anton Van Der Ven, Wanli Yang, and Louis F. J. Piper

J. Phys. Chem. C, **Just Accepted Manuscript** • DOI: 10.1021/acs.jpcc.9b01298 • Publication Date (Web): 07 May 2019

Distinction Between Intrinsic and X-ray Induced Oxidized Oxygen States in Li-rich 3d Layered Oxides and $LiAlO_2$

Zachary W. Lebens-Higgins,[†] Julija Vinckeviciute,[‡] Jinpeng Wu,[¶,§] Nicholas V. Faenza,[‖] Yixuan Li,[⊥] Shawn Sallis,[#] Nathalie Pereira,[‖] Ying Shirley Meng,[⊥] Glenn G. Amatucci,[‖] Anton Van Der Ven,[‡] Wanli Yang,[*,§] and Louis F. J. Piper[*,†]

†*Department of Physics, Applied Physics and Astronomy, Binghamton University, Binghamton, New York 13902, USA*

‡*Materials Department, University of California Santa Barbara, Santa Barbara, CA 93106, USA*

¶*Stanford Institute for Materials and Energy Sciences, Stanford University, Stanford, California 94305, United States*

§*Advanced Light Source, Lawrence Berkeley National Laboratory, Berkeley, California 94720, United States*

‖*Energy Storage Research Group, Department of Materials Science and Engineering, Rutgers University, North Brunswick, New Jersey 08902, United States*

⊥*Department of Nano Engineering, University of California San Diego (UCSD), La Jolla, California 92093, USA*

#*Materials Science & Engineering, Binghamton University, Binghamton, New York 13902, USA*

@*Materials Science & Engineering, Binghamton University, Binghamton, New York 13902, USA*

E-mail: wlyang@lbl.gov; lpiper@binghamton.edu

Abstract

Resonant inelastic x-ray scattering (RIXS) at the O K-edge is considered a prime technique to identify bulk oxidized oxygen formation but its fundamental interpretation is not straightforward. In this study, we intentionally induce RIXS signatures of oxidized oxygen upon beam exposure in $LiAlO_2$ polymorphs that are easily distinguished due to their wide band gaps. After careful consideration of beam exposure effects on LR-NMC ($Li[Li_{0.144}Ni_{0.136}Mn_{0.544}Co_{0.136}]O_2$), we conclude that oxidized oxygen features are inherent at high states of charge and are lost upon aggressive beam exposure. The extracted oxidized oxygen lineshapes from our x-ray irradiation studies for both $LiAlO_2$ (induced) and LR-NMC (inherent) are found to have an additional oxidized oxygen RIXS feature not observed in O_2 gas studies. This study highlights the unique insight of O K-edge RIXS into determining the nature and stability of oxidized oxygen states.

Introduction

Li-ion batteries have found widespread utilization in energy storage applications from consumer electronics to electric vehicles. Pursuit of higher energy densities has led to growing interest in Li-rich cathode materials.[1–4] Oxygen redox is widely considered to explain the higher obtainable capacities,[2,5–7] yet there remain limited probes of the oxygen

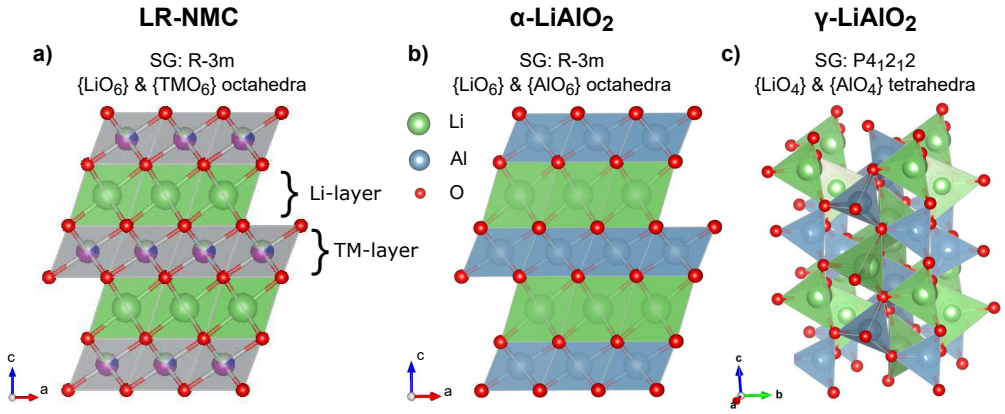

Figure 1: Crystal structures of a)$Li[Li_{0.144}Ni_{0.136}Mn_{0.544}Co_{0.136}]O_2$ (LR-NMC), b) α-$LiAlO_2$,[8] and c) γ-$LiAlO_2$.[8] The LR-NMC and α-$LiAlO_2$ are layered with a similar O3 stacking and octahedrally coordinated cations. The LR-NMC is shown in the R-3m space group (SG) along with the Ni/Co/Mn/Li ordering in the TM layer, though it is important to note these systems are often described with a C2/m SG relating to Mn-ordering in the TM-layer.[1]

environment to directly establish oxygen involvement.

Synchrotron x-ray sources provide unique insight into fundamental redox processes in cathode materials.[9,10] For alkali-rich systems, various O K-edge soft x-ray absorption (sXAS) studies[11–13] have relied on several peaks at energies of 528-531 eV as evidence of oxygen redox based on the Li_2O_2 $[O_2]^{2-}$ absorption peak in roughly the same energy range.[14] However, these peaks sit in the so-called "pre-edge" region of the O K-edge sXAS, which is dominated by transition-metal character.[10] O K-edge resonant inelastic x-ray scattering (RIXS) is considered a more reliable probe of bulk oxygen redox based on the emergence of a sharp feature observed at similar excitation/emission energies in a range of 3d transition metal (TM) systems, including Li-rich NMC,[7,15,16] $Na_{2/3}Mg_{1/3}Mn_{2/3}O_2$,[17] and $Li_{1.9}Mn_{0.95}O_{2.05}F_{0.95}$.[18] Although the origin of this feature in oxide cathodes remains uncertain, joint experiment and first principle simulations of the O K-edge RIXS of Li_2O_2 identified that such features are fundamentally defined by an O-2p intra-band excitation, which naturally requires unoccupied states in O-2p bands, i.e. oxidized oxygen.[19] Therefore, RIXS maps provide a reliable detection of the oxidized states in the oxide cathodes at high potentials.

Consideration of the stability of these oxygen environments in delithiated Li-rich systems during RIXS measurements is warranted as studies have shown the sensitivity of the oxidized oxygen states in Li_2O_2 to x-ray exposure.[14,19] Highly oxidized TM systems are known to be sensitive to radiation damage, such as Mn^{7+} in $KMnO_4$,[20] but there has been limited examination of x-ray exposure effects on Li-rich systems in these high flux experiments. This is particularly important for the Li-rich NMC systems that are known to lose oxygen during cycling[4,7,21] and upon irradiation, e. g. electron beam exposure.[22] $LiAlO_2$ provides a useful comparison of the exposure sensitivity of the oxygen environment as electron beam exposure tests have similarly observed beam induced oxygen loss.[23]

Here, we focus on two $LiAlO_2$ phases and $Li[Li_{0.144}Ni_{0.136}Mn_{0.544}Co_{0.136}]O_2$, a LR-NMC system, to evaluate x-ray exposure on the oxygen environment using O K-edge sXAS and RIXS. Irradiation tests on LR-NMC confirm the oxidized oxygen features are inherent at high states of charge, though these states are sensitive to aggressive beam exposure. The instability of oxidized oxygen to x-ray exposure in LR-NMC is contrasted with intentionally induced oxidized oxygen in LiAlO2. The surprising similarity of the extracted oxidized

oxygen RIXS lineshape for LR-NMC and γ-$LiAlO_2$ raises questions on the oxidized oxygen environments in each of these systems.

Methods

Synthesis

$Li[Li_{0.144}Ni_{0.136}Mn_{0.544}Co_{0.136}]O_2$ (LR-NMC) An aqueous solution containing $Ni(NO_3)_2{\cdot}6H_2O$, $Co(NO_3)_2{\cdot}6H_2O$ and $Mn(NO_3)_2{\cdot}4H_2O$ with a concentration of 1.0 M was pumped slowly to a reactor; at the same time, a 0.2 M Na_2CO_3 solution was added separately into the reactor. The pH value for the co-precipitation was fixed to 7.8. After reaction, the whole reactor was transferred into an oven and aged at 80 °C for 12 hours. The resulting $(Ni_{1/6}Co_{1/6}Mn_{4/6})CO_3$ powders were washed several times with distilled water, and dried in a vacuum oven at 80 °C overnight. The resulting precipitates were mixed with Li_2CO_3 and the exact molar ratio between them was 0.7. The mixed powders were first pre-heated at 500 °C for 5 hrs in air and then calcinated at 850 °C for 15 hrs in air. Heating speed was 5 °C/min. After calcination, they were cooled to room temperature. The LR-NMC system is described as either a solid solution in the $R\bar{3}m$ space group, which is shown in Figure. 1, or a two component system with Mn-local ordering in the C2/m space group based on the superstructure XRD peaks.

$LiAlO_2$ compounds α-LiAlO2 and γ-LiAlO2 were synthesized through co-precipitation of lithium acetate (Aldrich) and aluminum acetate basic hydrate (Alfa Aesar), which were mixed in stoichiometric amounts based on the precursors' metal content and dissolved in deionized water. As the mixture was continuously stirred, water was boiled off, and the resulting precipitate was dried for at least 16 hours at 60 °C in a dry room (dew point of -35 to -40 °C), and then ground in a fine powder with a mortar and pestle. The mixture was then annealed in an O_2 environment at 500 °C for 24 hrs to synthesize α-LiAlO2. γ-LiAlO2 was fabricated by reannealing the α-LiAlO2 material first at 850 °C for 48 hrs, and then again at 850 °C for 24 hrs. After each anneal the material was gradually cooled to room temperature and then finely ground with a mortar and pestle in a dry room. To prevent reaction of the material with moisture, immediately after synthesis the samples were stored in a dry room or inert (Ar) atmosphere. The γ-$LiAlO_2$ phase with space group $P4_12_12$ has a 3d-network structure consisting of LiO_4 and AlO_4 tetrahedra.[8] The α-$LiAlO_2$ phase with space group $R\bar{3}m$ is a layered structure consisting of LiO_6 and AlO_6 octahedra.[8] The α- and γ-$LiAlO_2$ structures are shown in Figure 1 alongside the LR-NMC for comparison.

Electrochemistry

Dried $Li[Li_{0.144}Ni_{0.136}Mn_{0.544}Co_{0.136}]O_2$ powder was mixed in an argon-filled glovebox with 5.0 wt % carbon black (SuperP, MMM) using a mortar and pestle. Powder cells (2032 Hohsen) were assembled using lithium metal (FMC) negative electrode with a combination of glass fiber (Whatman) and polyolefin (Celgard) seperators with 1 M LiPF6 ethylene carbonate:dimethyl carbonate (EC:DMC) (1:1 volume ratio) electrolyte (BASF). Half-cells containing the LR-NMC powder electrodes were charged at a constant current of 10 mA/g at 24 °C.

X-ray spectroscopy

Soft x-ray absorption spectroscopy (sXAS) and resonant inelastic x-ray scattering (RIXS) measurements were performed at the iRIXS endstation at beamline 8.0.1 at the Advanced Light Source with a beam size of 30 μm (V) x 100 μm (H)[24] and a range of flux controlled by entrance/exit slits. . Absorption spectra were collected in total electron yield (TEY) and total fluorescence yield (TFY) modes. For the long RIXS maps, we obtained a corresponding partial fluorescence yield absorption spectra from the integration of the emission associated with the element probed with the absorption edge. For energy calibration of the excitation

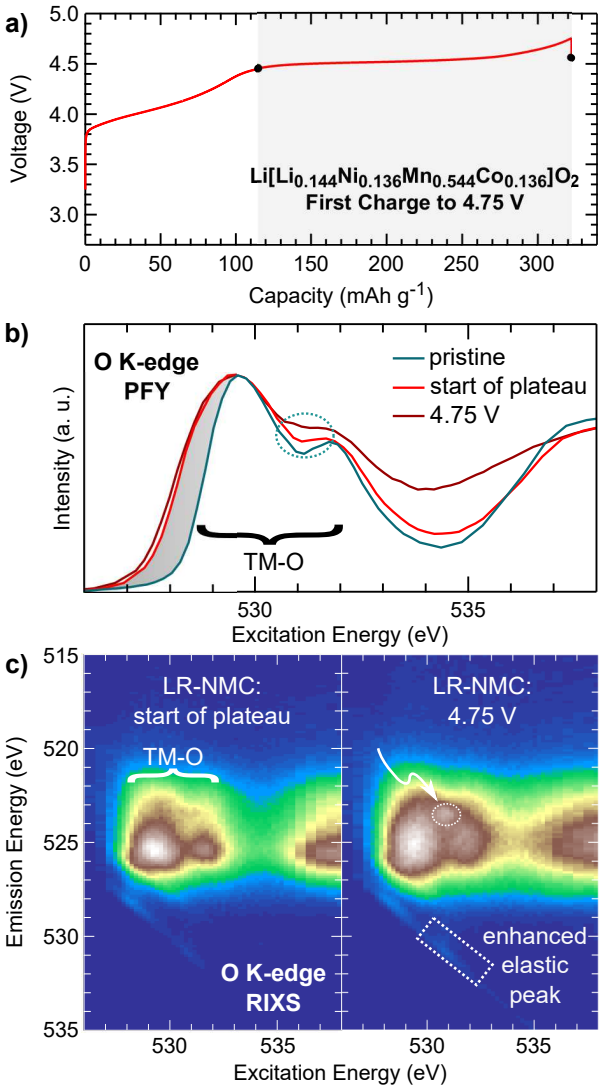

Figure 2: a) First charge of LR-NMC to 4.75 V at 10 mA g^{-1} and 24 °C. b) sXAS in PFY mode and c) RIXS maps of the O K-edge for LR-NMC electrodes charged to the start of the plateau (∼4.5 V/115 mAh g^{-1}) and to 4.75 V (322 mAh g^{-1}) as indicated in the electrochemical profile. The shading in the O K-edge PFY spectra reflects the nickel and cobalt oxidation that occurs before the start of the plateau. In the RIXS map, the oxidized oxygen feature and associated enhancement of the elastic peak are highlighted.

energy, a TiO2 reference was used for the O K- and Mn L-edges and a Ni metal reference was used for the Ni and Co L-edges. The emission energy was calibrated using the elastic peak in the map. For LR-NMC, powder electrodes extracted from coin-cells were used for the ex-situ RIXS measurements.

Density functional theory calculations

We used density functional theory (DFT) to calculate the energies and electronic band structures of α- and γ-LiAlO2, utilizing the Vienna Ab Initio Simulation Package (VASP)[25,26] with PAW pseudopotentials? and the optb86b-vdw functional.[27–30] The calculations were spin polarized, employed a 500 eV energy cutoff, and sampled the Brillouin zone with a k-point mesh density of at least 30 Å. Structures were first allowed to relax using Gaussian smearing until forces were converged to within 0.02 eV/$\AA$ and were then followed by static calculations using the tetrahedron method with Blöchl corrections[31] to obtain accurate energies and densities of state.

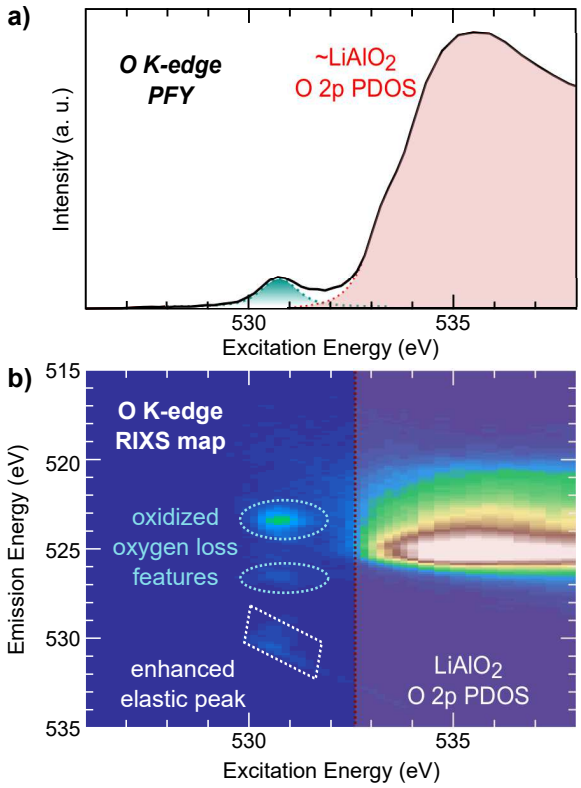

Figure 3: a) Bulk PFY spectra for γ-$LiAlO_2$ taken with 40/40 slits. b) Corresponding O K-edge RIXS map in which there are two sharp RIXS loss features and a strong elastic peak at 531 eV associated with oxidized oxygen states.

Results & Discussion

For the LR-NMC cathode selected for this study, the first charge profile is given in Fig. 2a. The first charge plateau is commonly associated with the activation of oxygen redox with multiple studies showing no evidence of further TM oxidation during this regime.[7,15–17] For the cutoff points indicated in the first charge, O K-edge measurements in bulk sensitive partial fluorescence yield (PFY) mode and RIXS maps are given in Fig. 2b-c. Corresponding Mn, Co, and Ni L_3-edge measurements for these electrodes, given in supplementary Fig. S1, do not show evidence of further TM oxidation. Between the start and end of the high voltage plateau, the PFY O K-edge absorption spectra shows only a small change in the pre-edge region (527 eV to 533 eV) in contrast to the clear change in lineshape observed between pristine and the start of charge associated with TM redox. For the RIXS maps of the LR-NMC electrodes, the features can be assigned to (i) the elastic line, which can include contributions from low-loss emission features such as phonons, (ii) emission from valence band states, and (iii) low-energy electron excitations.[10,32] More detailed discussion of each of these processes can be found in reviews by L. J. P. Ament et al.[32] and W. Yang and T. P. Devereaux.[10] After the high voltage plateau, a sharp emission feature, distinct from the broad TM-O hybridization features, is observed to emerge. There is a concurrent enhancement of the elastic peak associated with an increase in low-energy inelastic processes such as phonons. These features are highlighted for the 4.75 V LR-NMC electrode in Fig. 2. The emergence of these features along the high voltage plateau is consistent with previous RIXS of LR-NMC systems,[7,15–17] in which these features were assigned as signatures of oxidized oxygen. In Li_2O_2, a RIXS feature at the emission energy of the sharp feature (523.5 eV) was ascribed to an O 2p intra-band transition from occupied π_u states to unoccupied σ_u* states associated with oxidized oxygen.[19]

Using a similar x-ray flux and exposure time, we conducted O K-edge RIXS on γ-$LiAlO_2$. Bulk PFY absorption spectra and the corresponding RIXS map are given in Fig. 3. The PFY spectra above 532.5 eV is consistent with previous EELS spectra[23] and matches well to ground state density functional theory (DFT) calculations of the wide bandgap γ-$LiAlO_2$ system (Fig. S2).

The corresponding RIXS map for γ-$LiAlO_2$ in Fig 3 is broken up into two parts. At higher excitation energies ($>$ 532.5 eV), the spectra matches emission from O 2p valence band states (Fig. S2). When focusing on an excitation energy of 531 eV, we see three distinct features in the RIXS map associated with the PFY peak at 531 eV. There is an enhanced elastic peak and two sharp emission features at 523.5 and 526.5 eV, which are easily distinguished as there is no overlap with $LiAlO_2$ density of states features. The 523.5 eV feature matches the sharp feature observed for Li_2O_2, O_2, and LR-NMC, suggesting a similar assignment as oxidized oxygen. Interestingly, α-$LiAlO_2$, which has an O3 layered structure similar to LR-NMC,[8] also shows two loss features (Fig. S2).

As the presence of oxidized oxygen is unexpected in the as fabricated $LiAlO_2$, we conducted a more thorough sXAS exposure test of the O K-edge for the γ-$LiAlO_2$ system, given in Fig. 4. As shown in Fig. 3c, the x-ray flux was increased over the first 20 scans and decreased for the remaining scans. Select spectra in surface sensitive total electron yield (TEY) and bulk sensitive total fluorescence yield (TFY) mode are given in Fig. 4a-b. The initial TEY/TFY spectra (*scan 3*) match ground state DFT calculations of the O 2p partial density of states (PDOS), yet increasing the flux (*scan 9*) results in the emergence of the new ~531 eV peak in TEY/TFY. Surprisingly, after continued exposure (*scan 28*), the peak is absent in TEY mode but remains in TFY mode. From a detailed evaluation of the 531 eV peak intensity, given in Fig. 4c, we find a clear contrast between its formation and loss at the surface and persistence in the bulk. Complimentary RIXS measurements revealed the RIXS features were stable during extended x-ray exposure as well. From these

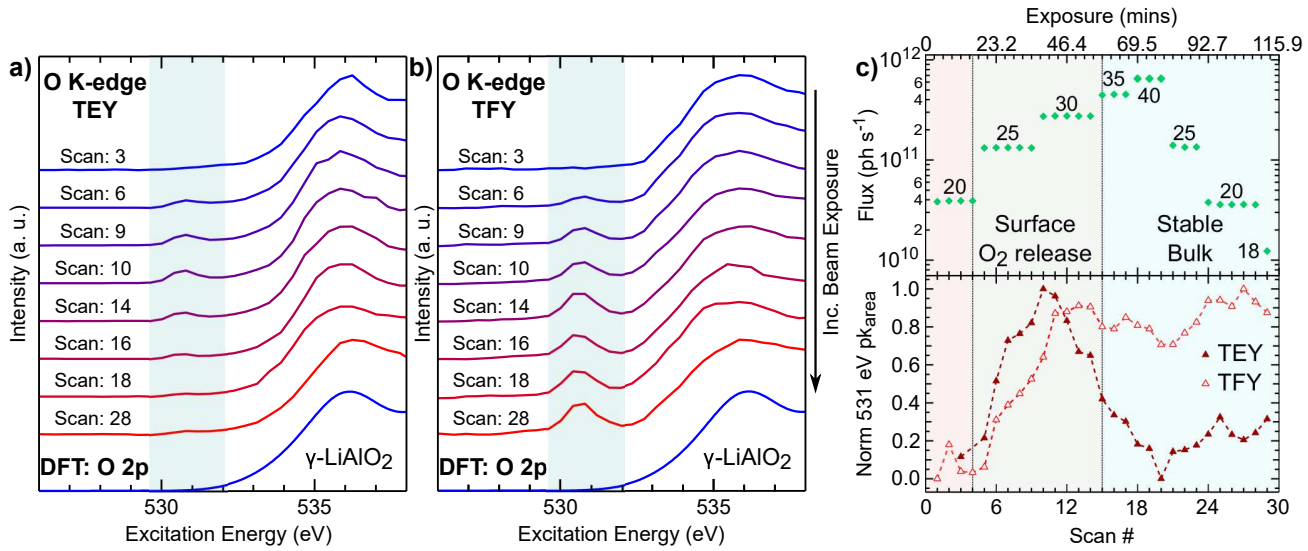

Figure 4: Select O K-edge (a) TEY and (b) TFY spectra from extended x-ray exposure test on the γ-$LiAlO_2$ system compared with ground state DFT calculations of the unoccupied O 2p PDOS. The beam induced peak at 531 eV is highlighted. c) Variation in flux and 531 eV peak in TEY and TFY mode for the 29 repeat scans. The flux was varied over an order of magnitude by changes in the entrance/exit slit width from 18/18 to 40/40 as indicated. The sample spot was exposed for ~4 mins during each scan for a total exposure time of 112 mins.

measurements, we can clearly assign the loss features to a new x-ray induced bulk phase (Figs. 2 & S5).

X-ray exposure tests were performed on the 4.75 V delithiated LR-NMC electrode to examine whether the oxidized oxygen states are intrinsic to this system. In Fig. 5, we compare x-ray exposure effects on the Ni L_3-edge sXAS and O K-edge sXAS and RIXS spectra taken at an excitation energy of 531 eV. The post-exposure O K-edge sXAS spectra was taken directly after the RIXS scans given in Fig. 5d. The Ni L_3-edge spectra were taken on a fresh spot with similar changes in flux (Fig. S3).

For the O K- and Ni L_3-edge sXAS spectra, we highlight changes associated with TM reduction at the surface due to beam exposure. In the Ni L_3-edge TEY spectra, there is an increase in the peak at 853 eV from S1 to S5 that is related to increased Ni^{2+}, which has significant weight at 853 eV compared to Ni^{3+} or Ni^{4+}.[33,34] Additional comparison of the Co L_3- and Mn L_3-edges reveal each of the TMs are partially reduced at the surface (Fig. S4). In the O K-edge TEY spectra, there is a concurrent decrease in the main pre-edge peak at 529 eV and growth of a peak at 532 eV. Based on the range of XAS/EELS studies of reduced surface phases for layered oxide cathodes,[3,35,36] these changes are consistent with the TM reduction. The limited changes of the O K- and Ni and Co L_3-edges in TFY mode indicate the x-ray induced TM reduction is restricted to the first few nms. This process is attributed to oxygen loss and formation of reduced surface phases as electron and x-ray damage often mimic the effects of long-term cycling.[22,37]

From scanning transmission x-ray microscopy measurements of LR-NMC, O K-edge features associated with oxidized oxygen were attributed to the particle bulk rather than the near-surface region,[15] so that TFY mode would provide increased sensitivity to these states. However, it is difficult to determine if bulk oxidized oxygen states are present/absent from TFY O K-edge spectra alone due to the overlap of TM-O hybridized states around 531 eV. Therefore, we employed continuous RIXS scans at an excitation energy of 531 eV to directly monitor the oxidized oxygen states. From

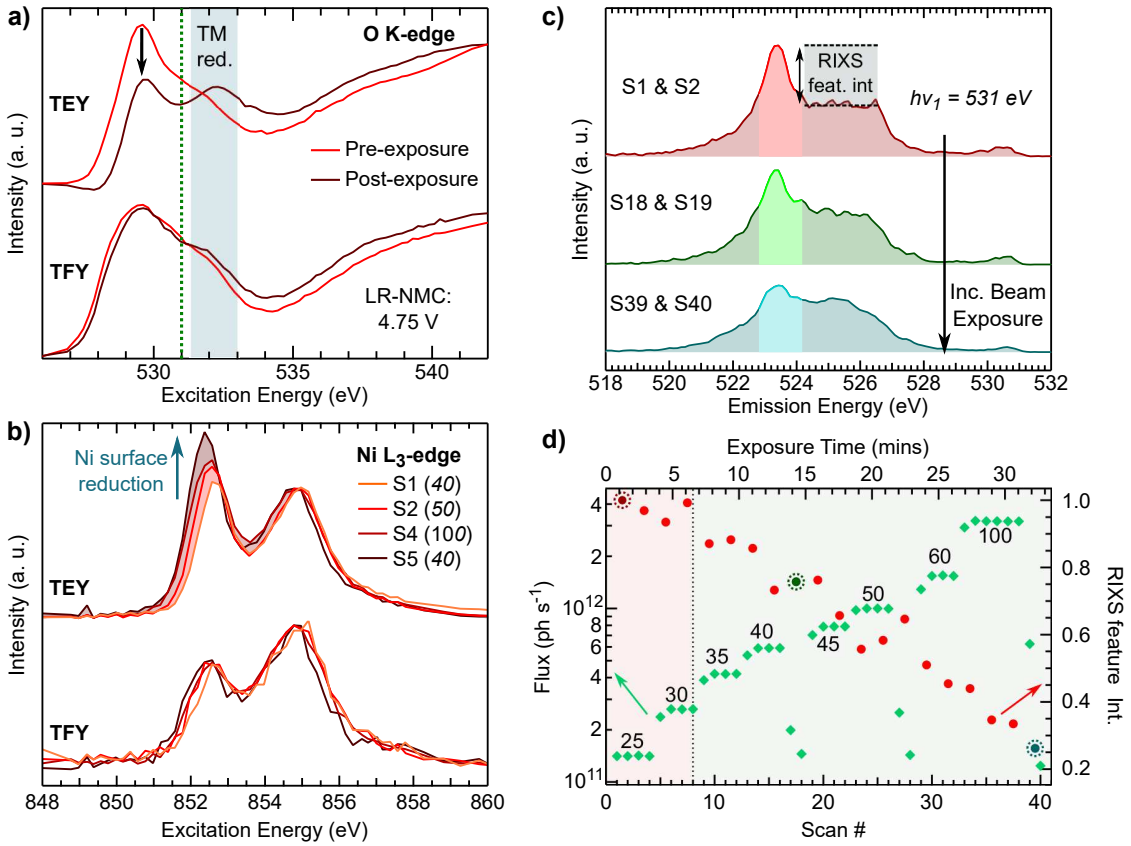

Figure 5: X-ray exposure tests for LR-NMC electrode charged to 4.75 V. a) O K-edge spectra taken pre/post- RIXS tests shown in part **c** & d. **b)** Repeat Ni L_3-edge scans. The induced nickel reduction is indicated in the TEY spectra. c-d) An extended exposure test of 40 RIXS scans taken at an excitation energy of 531 eV (dotted line in part **a**) for sensitivity to the oxidized oxygen states. Every two 45 sec scans are averaged to increase signal/noise. c) Select O K-edge RIXS spectra, each at 25/25 slits, to indicate the oxidized oxygen RIXS feature and changes with exposure/flux. d) Comparison of the flux and oxidized oxygen RIXS feature during the extended exposure test with entrance/exit slit values indicated.

the select RIXS scans presented in Fig. 5c, we find the strongest oxidized oxygen feature at the outset of the test and the lowest x-rary flux setting, i. e. with the minimum irradiation. Estimating the oxidized oxygen feature intensity throughout an extended exposure test (Fig. 5d), we found its intensity decreased relative to other features, with over a 50% loss during the 30 min test. The decrease in the oxidized oxygen feature was more prominent above 40/40 slits, though the extent of the radiation damage can be mitigated by scanning the x-ray across the sample surface during the measurement (Fig. S6). Therefore, opposite to the irradiation effect on $LiAlO_2$, the oxidized oxygen states in charged LR-NMC electrodes are suppressed with x-ray exposure.

There is no evidence of concurrent bulk TM reduction to maintain charge neutrality (Fig. 5b), even though there is a pronounced decrease in oxidized oxygen bulk states of LR-NMC. One possible explanation for this is that oxygen loss occurs with the concurrent reduction of non-divalent oxygen states to O^{2-}. In this case, the loss of oxygen would result in the formation of oxygen vacancies as has been reported upon cycling of Li-rich compounds.[3,4,38] A similar process may occur in the x-ray induced transformation of Li_2O_2 to Li_2O,[14,19] although more work is needed to evaluate this hypothesis. The stability of these oxidized oxygen states and any connection

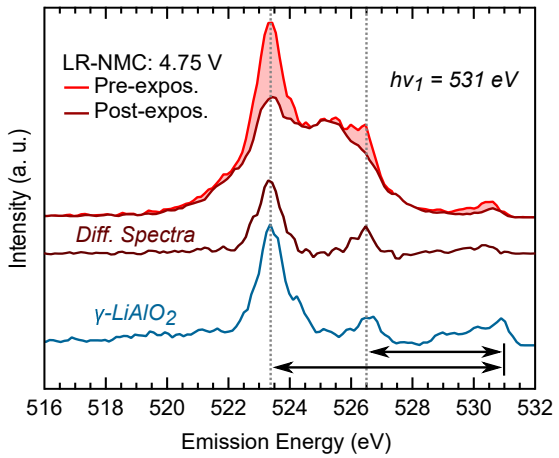

Figure 6: O K-edge RIXS cut at 531 eV for the LR-NMC charged to 4.75 V before and after x-ray exposure and for the x-ray induced state in γ-$LiAlO_2$. Difference spectra is given between the pre- and post-exposed LR-NMC to extract the oxidized oxygen RIXS lineshape. Grey dotted lines are used to highlight the emission energy of the RIXS features in the LR-NMC and γ-$LiAlO_2$ systems.

between lattice oxygen redox and concurrent oxygen gas release remain important questions for the Li-rich community.[2–4,10]

To comment on the non-divalent oxygen environments in LR-NMC and γ-$LiAlO_2$, we compare RIXS spectra sensitive to the oxidized oxygen features, given in Fig. 6. From our LR-NMC irradiation test, we extracted the RIXS lineshape associated with oxidized oxygen from the RIXS spectra for the first time. The difference spectra matches the two RIXS features observed for γ-$LiAlO_2$. First-principles simulations of the O K-edge RIXS of Li_2O_2 predicted two $[O_2]^{2-}$ features related to O 2p intra-band transitions at the σ_u*-absorption peak.[19] Although the O_2 gas π*-absorption peak is similarly at an excitation energy of ~531 eV, there is a single dominating RIXS feature at ~523 eV observed for O_2 gas.[39] For the LR-NMC system, it is interesting to find similar RIXS features to the simulations of Li_2O_2 system even though ex-situ Raman measurements of LR-NMC have not found evidence of an O-O separation comparable to Li_2O_2 (1.5 $\AA$).[7,40]

For understanding the formation of oxidized oxygen states in γ-$LiAlO_2$, we turn to a previous electron beam study that hypothesized the irradiation decomposition reactions based on observed structural changes as follows:[23]

$$5LiAlO_2 \rightarrow LiAl_5O_8 + O_2 \uparrow + 4Li \uparrow \quad (1)$$

$$4LiAl_5O_8 \rightarrow 10Al_2O_3 + O_2 \uparrow + 4Li \uparrow \quad (2)$$

In this study, an electron energy loss spectroscopy (EELS) peak at 531 eV was assigned to the O_2 gas release based on its formation and loss during electron beam exposure.[39] We attribute the similar evolution of the ~531 eV peak in our TEY measurements (Fig. 3a) to x-ray induced O_2 gas release from the surface. Given the limited structure of the TFY absorption spectra (Fig. 3b), it is difficult to distinguish from the sXAS alone whether the 531 eV peak relates to oxidized oxygen states or O_2 gas. The RIXS measurements overcome this ambiguity as the two RIXS features (Fig. 5) indicate the formation of bulk oxidized oxygen states that more closely resembles a peroxide. The newly formed environment in the $LiAlO_2$ bulk may be similar to intrinsic oxidized oxygen states in the amorphous Al_2O_3 that were reported to arise from O-O pairing (~1.5 $\AA$).[41] This elegantly highlights how RIXS can be used to distinguish between non-divalent oxygen states. We note this assignment is based primarily on the RIXS experiments and simulations of the Li_2O_2[19] and O_2 gas[42] systems, and hope this provokes modeling on other oxidized oxygen environment, especially in the much more complicated transition-metal oxides.

Conclusion

In conclusion, we have identified the importance of accounting for x-ray irradiation effects on the oxygen and transition metals. Surprisingly, aggressive x-ray irradiation results in an underestimation of the oxidized oxygen states in LR-NMC. This is in stark contrast to $LiAlO_2$ where the oxidized oxygen states are induced by aggressive x-rays. Our data provides direct evidence that the oxidized

oxygen environment is intrinsic to delithiated LR-NMC. Although RIXS has provided the most reliable probe to quantify oxidized oxygen states to date,[17] our work reveals how care is still needed in conducting RIXS measurements for quantitive analysis. Irradiation damage studies can be employed to extract the true RIXS lineshapes of oxygen redox candidates for directing the modeling of their oxidized oxygen environments.

Acknowledgement This work was supported as part of the NorthEast Center for Chemical Energy Storage (NECCES), an Energy Frontier Research Center funded by the U.S. Department of Energy, Office of Science, Office of Basic Energy Sciences under Award No. DE-SC0012583. The work at the ALS was supported by the Office of Basic Energy Sciences, of the U.S. Department of Energy under Contract No. DE-AC02-05CH11231. Z. W. L.-H. gratefully acknowledges support from a Doctoral Fellowship in Residence Award from the ALS.

Supporting Information Available

Supporting XAS and RIXS measurements conducted on the $LiAlO_2$ and LR-NMC systems along with details on the accumulated fluence for the radiation exposure tests.

References

(1) Qiu, B.; Zhang, M.; Xia, Y.; Liu, Z.; Meng, Y. S. Understanding and Controlling Anionic Electrochemical Activity in High-Capacity Oxides for Next Generation Li-Ion Batteries. *Chem. Mater.* **2017**, *29*, 908–915.

(2) Assat, G.; Tarascon, J.-M. Fundamental Understanding and Practical Challenges of Anionic Redox Activity in Li-ion Batteries. *Nat. Energy* **2018**, *3*, 373–386.

(3) Hu, E.; Yu, X.; Lin, R.; Bi, X.; Lu, J.; Bak, S.; Nam, K.-W.; Xin, H. L.; Jaye, C.; Fischer, D. A. et al. Evolution of Redox Couples in Li- and Mn-Rich Cathode Materials and Mitigation of Voltage Fade by Reducing Oxygen Release. *Nat. Energy* **2018**, *3*, 690–698.

(4) Singer, A.; Zhang, M.; Hy, S.; Cela, D.; Fang, C.; Wynn, T. A.; Qiu, B.; Xia, Y.; Liu, Z.; Ulvestad, A. et al. Nucleation of Dislocations and Their Dynamics in Layered Oxides Cathode Materials During Battery Charging. *Nat. Energy* **2018**, *3*, 641–647.

(5) Li, B.; Xia, D. Anionic Redox in Rechargeable Lithium Batteries. *Adv. Mater.* **2017**, *29*, 1701054.

(6) Seo, D.-H.; Lee, J.; Urban, A.; Malik, R.; Kang, S. The Structural and Chemical Origin of the Oxygen Redox Activity in Layered and Cation-Disordered Li-Excess Cathode Materials. *Nat. Chem.* **2016**, *8*, 692–697.

(7) Luo, K.; Roberts, M. R.; Hao, R.; Guerrini, N.; Pickup, D. M.; Liu, Y.-S.; Edström, K.; Guo, J.; Chadwick, A. V.; Duda, L. C. et al. Charge-Compensation in 3d-Transition-Metal-Oxide Intercalation Cathodes Through the Generation of Localized Electron Holes on Oxygen. *Nat. Chem.* **2016**, *8*, 1–17.

(8) Liu, G.; Liu, H. First Principles Study of $LiAlO_2$: New Dense Monoclinic Phase Under High Pressure. *J. Phys. Condens. Matter* **2018**, *30*, 115401.

(9) Wolf, M.; May, B. M.; Cabana, J. Visualization of Electrochemical Reactions in Battery Materials with X-ray Microscopy and Mapping. *Chem. Mater.* **2017**, *29*, 3347–3362.

(10) Yang, W.; Devereaux, T. P. Anionic and Cationic Redox and Interfaces in Batteries: Advances from Soft X-ray Absorption Spectroscopy to Resonant Inelastic Scattering. *J. Power Sources* **2018**, *389*, 188–197.

(11) Yabuuchi, N.; Takeuchi, M.; Nakayama, M.; Shiiba, H.; Ogawa, M.; Nakayama, K.; Ohta, T.; Endo, D.; Ozaki, T.; Inamasu, T. et al. High-Capacity Electrode Materials for Rechargeable Lithium Batteries: Li_3NbO_4-Based System with Cation-Disordered Rocksalt Structure. *Proc. Natl. Acad. Sci. U.S.A.* **2015**, *112*, 7650–7655.

(12) Oishi, M.; Yamanaka, K.; Watanabe, I.; Shimoda, K.; Matsunaga, T.; Arai, H.; Ukyo, Y.; Uchimoto, Y.; Ogumi, Z.; Ohta, T. Direct Observation of Reversible Oxygen Anion Redox Reaction in Li-Rich Manganese Oxide, Li_2MnO_3, Studied by Soft X-ray Absorption spectroscopy. *J. Mater. Chem. A* **2016**, *4*, 9293–9302.

(13) Mortemard de Boisse, B.; Liu, G.; Ma, J.; Nishimura, S.-i.; Chung, S.-C.; Kiuchi, H.; Harada, Y.; Kikkawa, J.; Kobayashi, Y.; Okubo, M. et al. Intermediate Honeycomb Ordering to Trigger Oxygen Redox Chemistry in Layered Battery Electrode. *Nat. Commun* **2016**, *7*, 11397.

(14) Qiao, R.; Chuang, Y. D.; Yan, S.; Yang, W. Soft X-Ray Irradiation Effects of Li_2O_2, Li_2CO_3 and Li_2O Revealed by Absorption Spectroscopy. *PLoS ONE* **2012**, *7*, 3–8.

(15) Gent, W. E.; Lim, K.; Liang, Y.; Li, Q.; Barnes, T.; Ahn, S.-J.; Stone, K. H.; Mcintire, M.; Hong, J.; Song, J. H. et al. Coupling Between Oxygen Redox and Cation Migration Explains Unusual Electrochemistry in lithium-Rich Layered Oxides. *Nat. Commun* **2017**, *8*, 2091.

(16) Xu, J.; Sun, M.; Qiao, R.; Renfrew, S. E.; Ma, L.; Wu, T.; Hwang, S.; Nordlund, D.; Su, D.; Amine, K. et al. Elucidating Anionic Oxygen Activity in Lithium-Rich Layered Oxides. *Nat. Commun* **2018**, *9*, 947.

(17) Dai, K.; Wu, J.; Zhuo, Z.; Li, Q.; Sallis, S.; Mao, J.; Ai, G.; Sun, C.; Li, Z.; Gent, W. E. et al. High Reversibility of Lattice Oxygen Redox Quantified by Direct Bulk Probes of Both Anionic and Cationic Redox Reactions. *Joule* **2018**,

(18) House, R. A.; Jin, L.; Maitra, U.; Tsuruta, K.; Somerville, J. W.; Förstermann, D. P.; Massel, F.; Duda, L.; Roberts, M. R.; Bruce, P. G. Lithium Manganese Oxyfluoride as a New Cathode Material Exhibiting Oxygen Redox. *Energy Environ. Sci.* **2018**, *11*, 926–932.

(19) Zhuo, Z.; Pemmaraju, C. D.; Vinson, J.; Jia, C.; Lee, I.; Sallies, S.; Li, Q.; Wu, J.; Dai, K.; Hussain, Z. et al. Spectroscopic Signature of Oxidized Oxygen States in Peroxides. *J. Phys. Chem. Lett* **2018**, *9*, 6378–6384.

(20) Van Schooneveld, M. M.; DeBeer, S. A Close Look at Dose: Toward L-edge XAS Spectral Uniformity, Dose Quantification and Prediction of Metal Ion Photoreduction. *J. Electron Spectrosc* **2015**, *198*, 31–56.

(21) Qiu, B.; Zhang, M.; Wu, L.; Wang, J.; Xia, Y.; Qian, D.; Liu, H.; Hy, S.; Chen, Y.; An, K. et al. Gas-Solid Interfacial Modification of Oxygen Activity in Layered Oxide Cathodes for Lithium-Ion Batteries. *Nat. Commun* **2016**, *7*, 1–10.

(22) Lu, P.; Yan, P.; Romero, E.; Spoerke, E. D.; Zhang, J.-G.; Wang, C.-M. Observation of Electron-Beam-Induced Phase Evolution Mimicking the Effect of the Charge-Discharge Cycle in Li-Rich Layered Cathode Materials Used for Li Ion Batteries. *Chem. Mater.* **2015**, *27*, 1375–1380.

(23) Hetaba, W.; Mogilatenko, A.; Neumann, W. Electron Beam-Induced Oxygen Desorption in γ-$LiAlO_2$. *Micron* **2010**, *41*, 479–483.

(24) Qiao, R.; Li, Q.; Zhuo, Z.; Sallis, S.; Fuchs, O.; Blum, M.; Weinhardt, L.;

Heske, C.; Pepper, J.; Jones, M. et al. High-Efficiency In Situ Resonant Inelastic X-ray Scattering (iRIXS) Endstation at the Advanced Light Source. *Rev. Sci. Instrum.* **2017**, *88*.

(25) Kresse, G.; Furthmüller, J. Efficient Iterative Schemes for Ab Initio Total-Energy Calculations Using a Plane-Wave Basis Set. *Phys. Rev. B* **1996**, *54*, 11169–11186.

(26) Kresse, G.; Furthmüller, J. Efficiency of Ab-Initio Total Energy Calculations for Metals and Semiconductors Using a Plane-Wave Basis Set. *Comput. Mater. Sci.* **1996**, *6*, 15 – 50.

(27) Klimeš, J.; Bowler, D. R.; Michaelides, A. Chemical Accuracy for the Van Der Waals Density Functional. *J. Phys. Condens. Matter* **2009**, *22*, 022201.

(28) Dion, M.; Rydberg, H.; Schröder, E.; Langreth, D. C.; Lundqvist, B. I. Van der Waals Density Functional for General Geometries. *Phys. Rev. Lett.* **2004**, *92*, 246401.

(29) Román-Pérez, G.; Soler, J. M. Efficient Implementation of a Van Der Waals Density Functional: Application to Double-Wall Carbon Nanotubes. *Phys. Rev. Lett.* **2009**, *103*, 096102.

(30) Klimeš, J. C. V.; Bowler, D. R.; Michaelides, A. Van Der Waals Density Functionals Applied to Solids. *Phys. Rev. B* **2011**, *83*, 195131.

(31) Blöchl, P. E.; Jepsen, O.; Andersen, O. K. Improved Tetrahedron Method for Brillouin-Zone Integrations. *Phys. Rev. B* **1994**, *49*, 16223–16233.

(32) Ament, L. J. P.; Van Veenendaal, M.; Devereaux, T. P.; Hill, J. P.; Van Den Brink, J. Resonant Inelastic X-ray Scattering Studies of Elementary Excitations. *Rev. Mod. Phys.* **2011**, *83*, 705–767.

(33) Koyama, Y.; Mizoguchi, T.; Ikeno, H.; Tanaka, I. Electronic Structure of Lithium Nickel Oxides by Electron Energy Loss Spectroscopy. *J. Phys. Chem. B* **2005**, *109*, 10749–10755.

(34) Qiao, R.; Liu, J.; Kourtakis, K.; Roelofs, M. G.; Peterson, D. L.; Duff, J. P.; Deibler, D. T.; Wray, L. A.; Yang, W. Transition-Metal Redox Evolution in $LiNi_{0.5}Mn_{0.3}Co_{0.2}O_2$ Electrodes at High Potentials. *J. Power Sources* **2017**, *360*, 294–300.

(35) Hwang, S.; Kim, D. H.; Chung, K. Y.; Chang, W. Understanding Local Degradation of Cycled Ni-Rich Cathode Materials at High Operating Temperature for Li-Ion Batteries. *Appl. Phys. Lett.* **2014**, *105*, 103901.

(36) Yoon, W. S.; Haas, O.; Muhammad, S.; Kim, H.; Lee, W.; Kim, D.; Fischer, D. A.; Jaye, C.; Yang, X. Q.; Balasubramanian, M. et al. In Situ Soft XAS Study on Nickel-Based Layered Cathode Material at Elevated Temperatures: a Novel Approach to Study Thermal Stability. *Sci. Rep.* **2014**, *4*, 6827.

(37) Radin, M. D.; Hy, S.; Sina, M.; Fang, C.; Liu, H.; Vinckeviciute, J.; Zhang, M.; Whittingham, M. S.; Meng, Y. S.; Van der Ven, A. Narrowing the Gap Between Theoretical and Practical Capacities in Li-Ion Layered Oxide Cathode Materials. *Adv. Energy Mater.* **2017**, *7*, 1602888.

(38) Rana, J.; Kloepsch, R.; Li, J.; Stan, M.; Schumacher, G.; Winter, M.; Banhart, J. Structural Changes in a Li-Rich $0.5Li_2MnO_3$*$0.5LiMn_{0.4}Ni_{0.4}Co_{0.2}O_2$ Cathode Material for Li-Ion Batteries: A Local Perspective. *J. Electrochem. Soc.* **2016**, *163*, A811–A820.

(39) Hennies, F.; Pietzsch, A.; Berglund, M.; Föhlisch, A.; Schmitt, T.; Strocov, V.; Karlsson, H. O.; Andersson, J.; Rubensson, J. E. Resonant Inelastic

Scattering Spectra of Free Molecules with Vibrational Resolution. *Phys. Rev. Lett.* **2010**, *104*, 1–4.

(40) Ruther, R. E.; Callender, A. F.; Zhou, H.; Martha, S. K.; Nanda, J. Raman Microscopy of Lithium-Manganese-Rich Transition Metal Oxide Cathodes. *J. Electrochem. Soc.* **2014**, *162*, A98–A102.

(41) Arhammar, C.; Pietzsch, A.; Bock, N.; Holmstrom, E.; Araujo, C. M.; Grasjo, J.; Zhao, S.; Green, S.; Peery, T.; Hennies, F. et al. Unveiling the Complex Electronic Structure of Amorphous Metal Oxides. *Proc. Natl. Acad. Sci. U.S.A.* **2011**, *108*, 6355–6360.

(42) Ruckman, M. W.; Chen, J.; Qiu, S. L.; Kuiper, P.; Strongin, M.; Dunlap, B. I. Interpreting the Near Edges of O_2 and O_2^- in Alkali-Metal Superoxides. *Phys. Rev. Lett.* **1991**, *67*, 2533–2536.

Graphical TOC Entry